Mapping gravitational lens systems B2045+265 and B1608+656 in the radio spectrum

C. E. Flack

Abstract

We map radio observations of gravitational lens systems B2045+265 and B1608+656 with the Very Long Baseline Array and find precise positions of the lens components in both systems, as well as the radio-loud lensing galaxy in B2045+265. We also detect possible extended structure in the strongest lens component of B2045+265, but are unable to create a spectrum since the system was only observed at 5.0 GHz. B1608+656 was observed at four frequencies, 1.6, 5.0, 8.4 and 15.0 GHz, allowing us to create a spectrum of the source.

1. Introduction

Gravitational lensing is the process in which light from a distant source is bent toward an observer by an object in the same line of sight as the observer and source. Differences in the mass of the lens and the distance between the lens and source result in three categories of gravitational lensing: strong, weak and microlensing. Strong gravitational lensing is the result of the light from a source, usually a quasar, being lensed by a massive object, such as a galaxy, resulting in multiple images. Each lensed image is distorted and magnified while still conserving surface brightness. The process that creates weak gravitational lensing is essentially the same as strong gravitational lensing, however, the distance between the source and the lens is too great to result in multiple images. Microlensing is once again similar, but the lensing objects in this case are very compact. These lenses generally consist of individual stars or Massive Compact Halo Objects (MACHOs), resulting in small but noticeable distortions or magnifications of the source image. Radio wavelengths are generally not affected by microlensing because the emitting region is much larger than the lensing object, but optical through x-ray data are prone to the effects of microlensing. In each case, the light from the source is distorted and magnified, giving us a rare opportunity to examine both the source and the lens.

Gravitational lensing is a relatively new tool available to cosmologists which can be used to examine many aspects of the universe. Very distant objects, such as high redshift galaxies, normally can not be seen by local telescopes, but the natural magnification of gravitational lensing conserves surface brightness, giving us a rare opportunity to explore the structure of these distant objects.

Strong gravitational lensing gives us another powerful tool to measure the Hubble constant (H_0) directly, unlike other methods which require several assumptions. In strong gravitational lens systems with variable sources, the time delay between intensity changes in the images can be measured by simply observing the system. The delays are due to the differences in path lengths taken by the light, called the geometric delay, and a general relativistic effect due to light passing through the strong potential well of the lensing galaxy, called the gravitational delay. These values can be used, along with the mass distribution of the lens to determine the expansion rate of the universe.

Strong gravitational lensing can also be used to determine the mass distribution of a lensing galaxy. Detecting the distortion of extended structure in the lens components is evidence of small scale irregularities in the lensing galaxy. These distortions, as well as the positions and brightnesses of the lens components and an accurate position of the lensing galaxy are very strong constraints on the model of the lensing galaxy's mass profile.

The detection of extended structure in lens components is dependent on the angular resolution (θ) of the telescope, which is a function of the diameter (D) of the primary collecting surface, where $\theta \propto 1/D$. Radio interferometers, or simply arrays of radio telescopes, are capable of very high angular resolution because the longest baseline determines the resolution of the array. The Very Large Array (VLA) in New Mexico consists of 27 radio telescopes with a longest baseline between 1-30km, depending on the configuration. Even in its widest configuration, the VLA has an angular resolution of arcseconds. The Very Long Baseline Array (VLBA) consists of ten radio telescopes scattered across the United States, including one in Hawaii and one in St. Croix, and has an angular resolution on the order of milliarcseconds.

2. Calibration and Imaging

The VLBA data for B2045+265 and B1608+656 were calibrated in Astronomical Image Processing System (AIPS) using the pipeline VLBAPIPE, which took a multi-source file, calibrated the data and split the data into individual files. The single-source files were then mapped using IMAGR to produce wide field dirty maps of the lens systems. Fields were defined around each image component and the locations of the lensing galaxies and used when running subsequent iterations of IMAGR to expedite the process.

2.1 *B2045+265*

After flagging the data and creating a set of shallow clean maps with IMAGR, the 5.0-GHz observations of B2045+265 were phase-only self-calibrated using a 10 minute solution interval. The self-calibrated data was then cleaned to 2 times the map rms, self-calibrated again with a 10 minute solution interval, then cleaned to 2 times the rms to produce the final maps. See Figure 1 for a wide field VLA map of the system and Figure 2 for the VLBA fields of each lens component and the lensing galaxy.

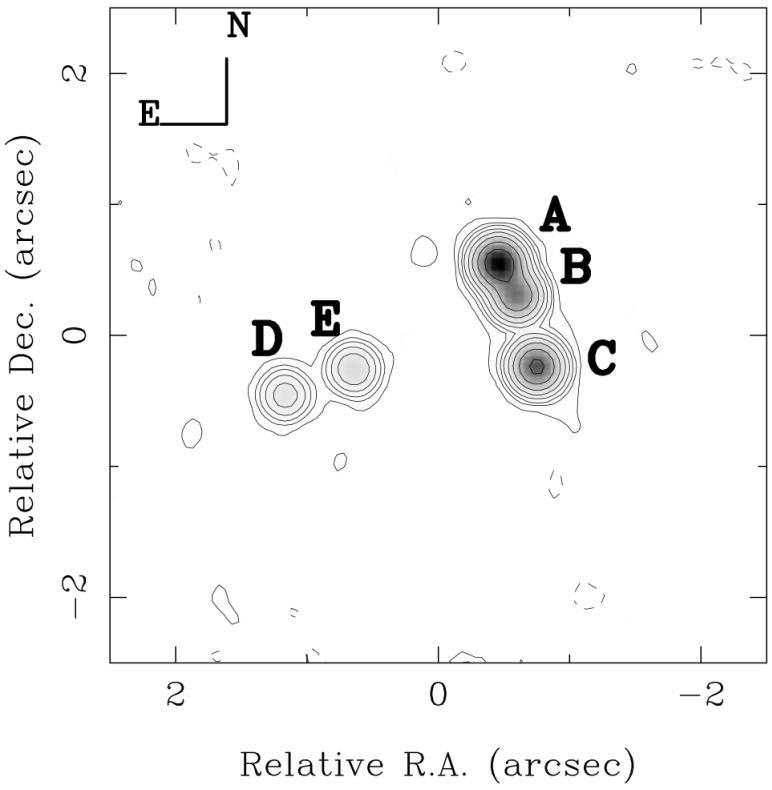

Figure 1. VLA 8.5-GHz observation of B2045+265 taken 1996 December (Fassnacht et al. 1999).

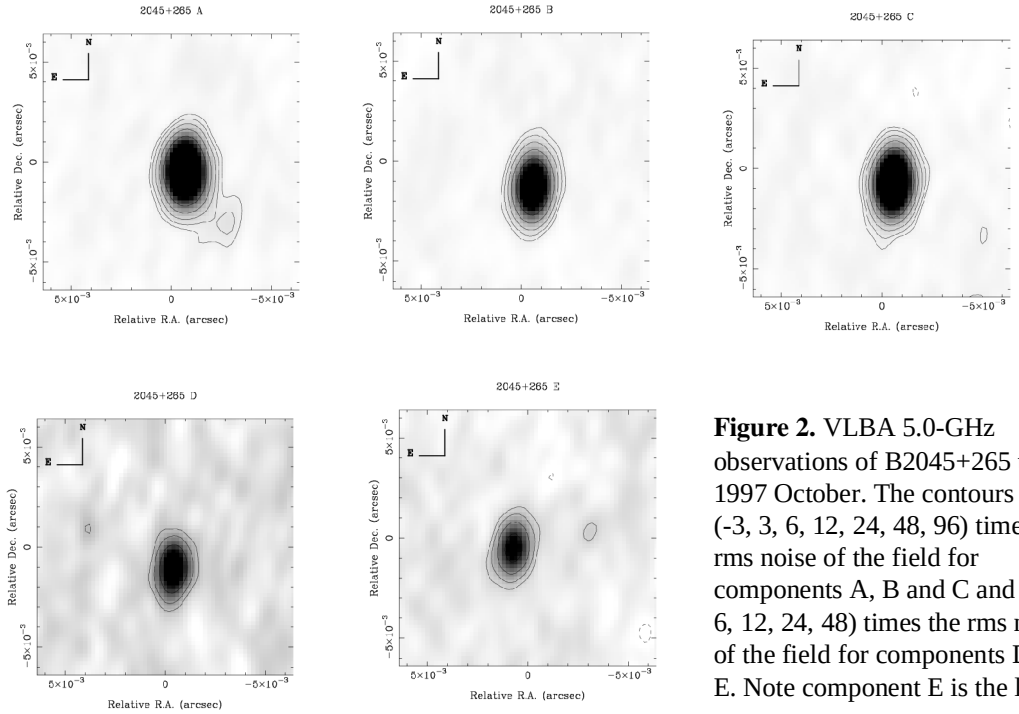

Figure 2. VLBA 5.0-GHz observations of B2045+265 taken 1997 October. The contours are (-3, 3, 6, 12, 24, 48, 96) times the rms noise of the field for components A, B and C and (-3, 3, 6, 12, 24, 48) times the rms noise of the field for components D and E. Note component E is the lensing galaxy.

2.2 *B1608+656*

B1608+656 was observed at 1.6, 5.0, 8.4 and 15.0 GHz. A dirty map of the 8.4-GHz observations was created with IMAGR and UVPLT was used to look at the initial uncalibrated data. The observations were a combination of VLBA and Effelsberg observations. Unfortunately, due to a problem with the collection of the Effelsberg data, they could not be calibrated and were deleted from the data set. The flagged data were run through VLBAPIPE again and mapped. Phase-only self-calibration was run three times, using 10, 10 and 5 minute solution intervals, and cleaning to two times the rms after each self-calibration.

Similar iterations of self-calibration and cleaning were done with the 5.0 and 15.0-GHz data. For the 5.0-GHz data, solution intervals of 10, 10 and 3 minutes were used, while the 15.0-GHz data were calibrated with 10, 10, 5 and 3 minute solution intervals. The 1.6-GHz data had already been split into a single source file and partially analyzed, so the data were cleaned and imaged using IMAGR but no other calibration was done. See Figure 3 for 8.4-GHz VLA observations of the system and Figure 4 for images of the lens components at 8.4 GHz taken with the VLBA.

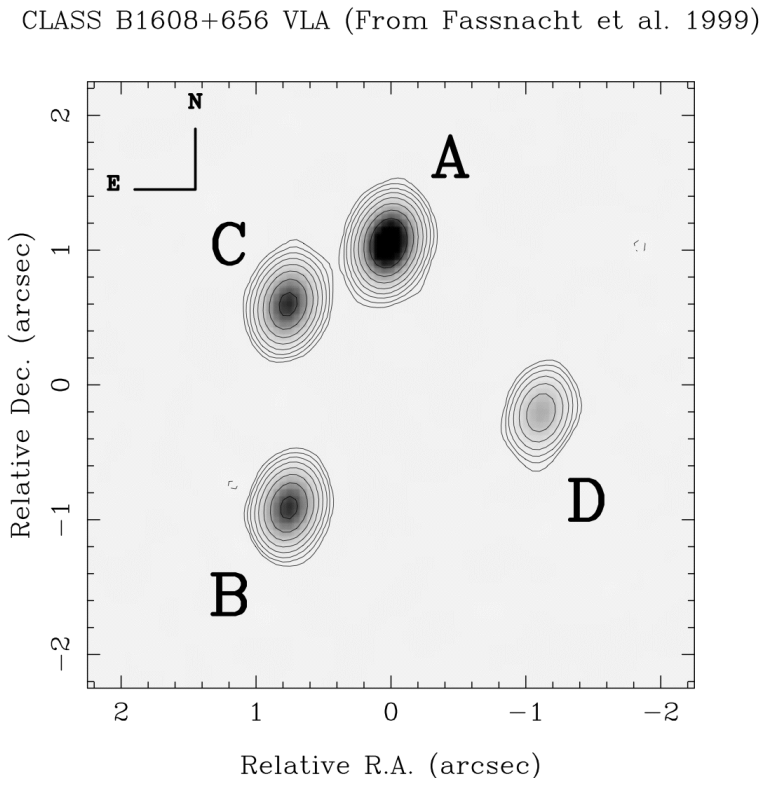

Figure 3. B1608+656 from VLA observations at 8.4 GHz. Note the absence of the lensing galaxies.

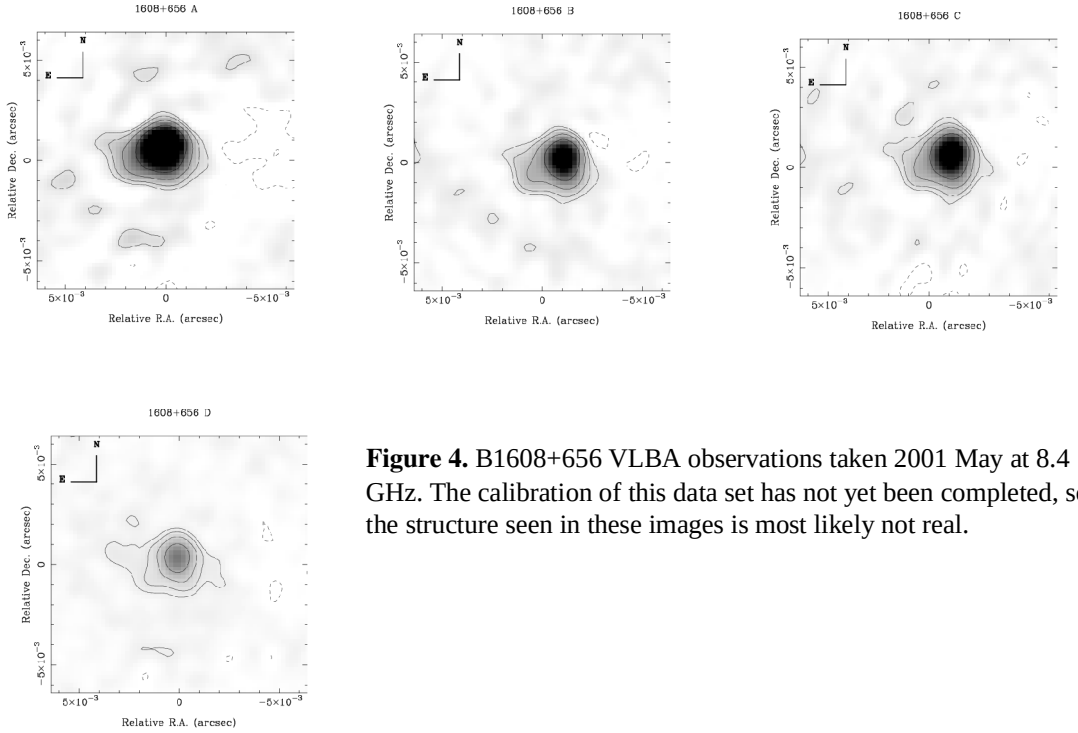

Figure 4. B1608+656 VLBA observations taken 2001 May at 8.4 GHz. The calibration of this data set has not yet been completed, so the structure seen in these images is most likely not real.

3. Data & Discussion

The final maps were fitted with Gaussian models using JMFIT. For B2045+265, component A was fitted with two Gaussian functions, representing the compact core and the extended emission, respectively. Components B, C, D and E were fitted with a single Gaussian each, implying no extended structure was detected. Table 1 shows the flux densities for B2045+265. Since the system was only observed at 5.0 GHz a spectrum could not be created, but a plot of the intensities from the VLBA data compared to previous observations of the system with the VLA at 4.9 GHz (Fassnacht et al. 1999) is shown in Figure 5.

TABLE 1
Component Flux Densities

Date	Array	ν (GHz)	S_A (mJy)	S_B (mJy)	S_C (mJy)	S_D (mJy)	S_E (mJy)	RMS (mJy beam^{-1})
1996 Dec 31	VLA	4.9	23.40	12.65	15.19	2.68	3.00	0.06
1997 Oct 17	VLBA	5.0	*14.543 +/- 0.081	9.166 +/- 0.112	14.042 +/- 0.109	1.595 +/- 0.103	1.762 +/- 0.092	0.055

* The best fit for Component A was two Gaussians. The fluxes of the two functions were simply added together, with the error added in quadrature.

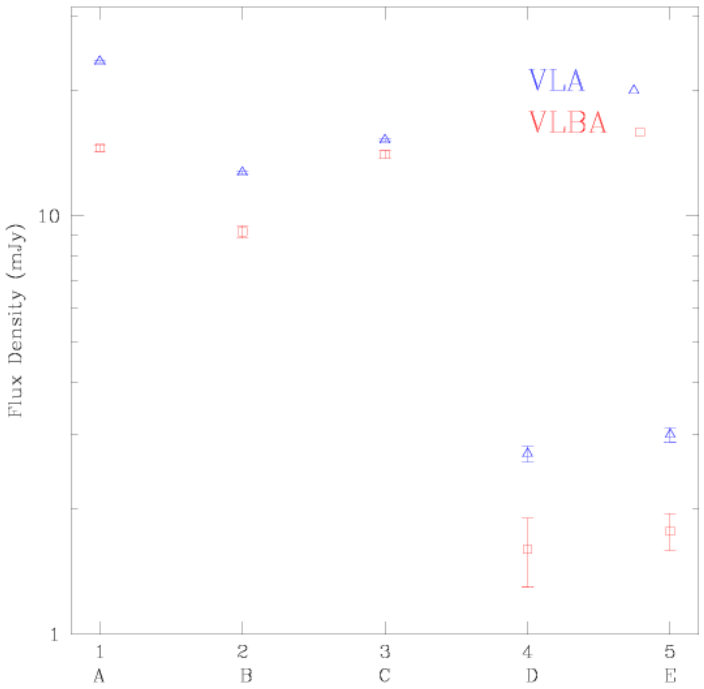

Figure 5. Comparison of the flux densities observed by the VLA in 1996 December at 4.9 GHz with those taken by the VLBA in 1997 September at 5.0 GHz. The error bars for the VLA data are 3σ from the rms noise of the map, while the error bars for the VLBA data are from the model fit errors.

After the calibration and mapping of B1608+656, JMFIT was run on the final maps and the resulting flux densities are shown in Table 2. Most of the objects fitted two Gaussian functions, but still looked essentially like point sources in the maps. Due to the higher angular resolution of the 15.0-GHz observations, extended emission is detected in all of the lensed images and flips directions between three of the components. The radio spectra of B1608+656, seen in Figure 6, are consistent with each other, with the exception of the lower frequency observations in component C. This inconsistency can clearly be seen in Figure 7, showing the flux density ratios with respect to component A.

TABLE 2
Component Flux Densities

ν (GHz)	Date	S_A (mJy)	S_B (mJy)	S_C (mJy)	S_D (mJy)	RMS (mJy beam^{-1})
1.6	1996 Apr 12	18.326 +/- 0.19	9.276 +/- 0.20	6.213 +/- 0.17	3.259 +/- 0.11	0.06
5.0	1995 Aug 20	38.565 +/- 0.61	19.300 +/- 0.40	18.379 +/- 0.37	6.947 +/- 0.36	0.58
8.4	2001 May 01	16.779 +/- 0.50	8.764 +/- 0.33	9.810 +/- 0.35	3.867 +/- 0.37	0.10
15.0	1995 Aug 20	24.135 +/- 1.7	16.182 +/- 2.3	18.819 +/- 2.7	7.426 +/- 2.8	0.18

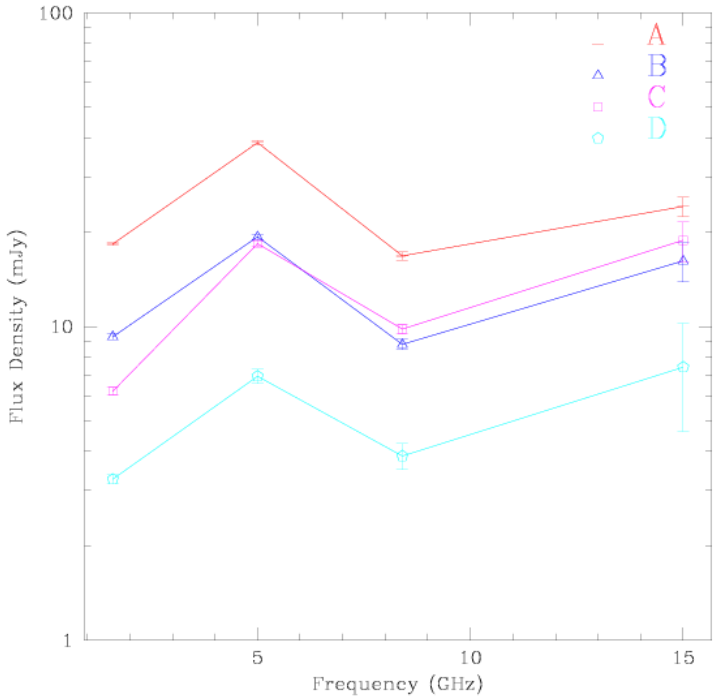

Figure 6. Radio Spectra of B1608+656 with 3σ error bars from the rms noise of the final maps.

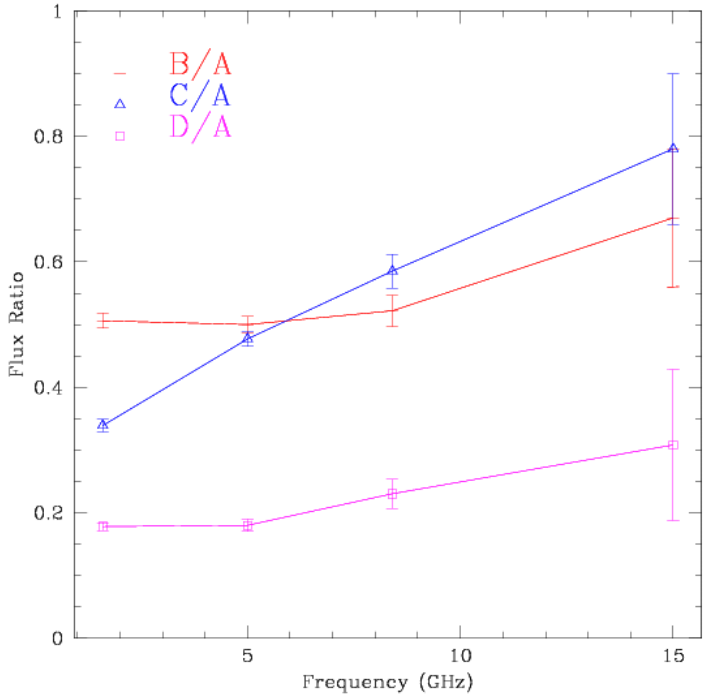

Figure 7. Flux density ratios for B1608+656 with respect to component A. Error bars are the rms noise of the final maps with respect to the ratios.

TABLE 3
Component Flux Density Ratios

ν (GHz)	Date	B/A	C/A	D/A
1.6	1996 Apr 12	18.326 +/- 0.19	9.276 +/- 0.20	6.213 +/- 0.17
5.0	1995 Aug 20	38.565 +/- 0.61	19.300 +/- 0.40	18.379 +/- 0.37
8.4	2001 May 01	16.779 +/- 0.50	8.764 +/- 0.33	9.810 +/- 0.35
15.0	1995 Aug 20	24.135 +/- 1.7	16.182 +/- 2.3	18.819 +/- 2.7

4. Conclusions & Further Work

A small amount of extension was found in the brightest component of B2045+265, but no modeling of the system can be done since this structure is not observed in any of the other lens components. Component D, the weakest lens component had not been detected in previous VLBA observations, but a precise position for component D, as well as the other lens components and the lensing galaxy were determined.

Due to problems with the Effelsberg data, the angular resolution of the 8.4-GHz observations of B1608+656 was lost, resulting in no detection of extended structure. Structure was not found in the 1.6 and 5.0-GHz data either, though the models fit two Gaussians to the maps. The higher resolution of the 15.0-GHz data did result in the detection of extended emission and clear flipping of the images. For any further research to be done on these systems they must first be observed with higher angular resolution in order to detect the extended emission. This will allow more accurate models of the lensing galaxies' mass distributions to be created.

We would like to thank Chris Fassnacht, John McKean and Matthew Auger for constant advise and guidance throughout the summer. Also, thanks to Rena Zieve for organizing and coordinating the UC-Davis REU program and the National Science Foundation for funding a program which gives undergraduates the opportunity to experience research in physics.

References

Fassnacht, C. D., et all. 1999, ApJ, 117, 658
Koopmans, L. V. E., et al. 2003, ApJ, 599, 70
Rusin, D., et al. 2002, MNRAS, 330, 205